# Joint Inversion of Reflectivity and Background subsurface components (JIRB)

*Alejandro Cabrales-Vargas*

## ABSTRACT

I perform a joint inversion for the reflectivity and background components of the subsurface. I pose this method as an optimization problem that is linear with respect to the reflectivity component, and non-linear with respect to the background component, therefore becoming overall nonlinear. Feasible solutions are confined to background models that drive the migration image to maximum focusing. The latter is achieved by maximizing the energy of the migration image in a second functional. The numerical results demonstrate that the method can recover a corrected reflectivity value.

## INTRODUCTION

Joint inversion of the reflectivity and background subsurface components is usually thought as a full waveform inversion (FWI) problem (Tarantola, 1984; Virieux and Operto, 2009) where no fundamental difference between such components is assumed, i.e., both of them are "bundled" within the same subsurface model. The factual recovery of such a "complete" subsurface model is arguably one of the most ambitious goals in seismic exploration.

I have been working on a different (and less ambitious) problem that consists of inverting for both components of the subsurface model, reflectivity and background, separately. What I mean by "separately" is that they are regarded as different parameter sets, rather than a single one as it is the case of FWI. Initially I had intended to set the problem as a linear optimization, which I had initially named Linearized Waveform Inversion with Velocity Updating (LWIVU) (e.g. Cabrales-Vargas et al., 2017; Cabrales-Vargas, 2017, 2018). This technique would in principle succeed if we included a term in the objective function that enforces maximization of energy of the migration image. However, in the last SEP report (Cabrales-Vargas and Sarkar, 2019) it was proved that a linearized version of such a term does not actually have a maximum, hence making futile further efforts towards getting meaningful results from such a particular inversion. One way to fix this problem is keeping the migration image nonlinear with respect to the background subsurface model for this term. Cabrales-Vargas and Sarkar (2019) proposed precisely that. In this report I take a step forward and make the image nonlinear in both terms, obtaining

$$\Phi(\mathbf{r},\mathbf{b}) = \frac{1}{2}\|\mathbf{H}(\mathbf{b}_0)\mathbf{r} - \mathbf{I}(\mathbf{b})\|_2^2 - \frac{\lambda}{2}\|\mathbf{I}(\mathbf{b})\|_2^2, \tag{1}$$

where $\mathbf{H}(\mathbf{b}_0)\mathbf{r}$ is the Gauss-Newton Hessian of FWI evaluated at the wrong background, $\mathbf{b}_0$, applied to the reflectivity, $\mathbf{r}$, and $\mathbf{I}(\mathbf{b})$ is the migration image evaluated at the inverted background, $\mathbf{b}$. The parameter $\lambda$ balances the importance of each functional, and the minus sign allows the maximization of the second functional within the minimization problem. As I will discuss later, this method assesses relatively small inaccuracies in the background model.

In the next section I provide a brief derivation of equation (1) and its gradient. Next, I provide numerical results. Finally I present the conclusions of this report.

## METHOD

Cabrales-Vargas and Sarkar (2019) provide a complete derivation of the JIRB problem, which in its general form is given by

$$\Phi(\mathbf{r},\mathbf{b}) = \frac{1}{2}\|\mathbf{H}(\mathbf{b})\mathbf{r} - \mathbf{I}(\mathbf{b})\|_2^2 - \frac{\lambda}{2}\|\mathbf{I}(\mathbf{b})\|_2^2. \tag{2}$$

The difference between equations (1) and (2) is that the former has been simplified by dropping second and higher order terms from the following expansion:

$$\mathbf{H}(\mathbf{b}_0 + \boldsymbol{\Delta}\mathbf{b})\mathbf{r} = \mathbf{H}(\mathbf{b}_0)\mathbf{r} + O(\boldsymbol{\Delta}\mathbf{b},\mathbf{r}), \tag{3}$$

where $\mathbf{b} = \mathbf{b}_0 + \boldsymbol{\Delta}\mathbf{b}$ and $\boldsymbol{\Delta}\mathbf{b}$ represents a perturbation in the background. Note that "high order terms" refers to terms containing both parameters. For sufficiently small values of $\boldsymbol{\Delta}\mathbf{b}$ and $\mathbf{r}$ (the latter by definition is small) we can justify dropping the high order terms that compound $O(\boldsymbol{\Delta}\mathbf{b},\mathbf{r})$. Numerical experiments (not included in this report) also justify this approximation. For this reason, it must be emphasized that the method assumes the presence of relatively small inaccuracies in the background.

The objective function proposed by Cabrales-Vargas and Sarkar (2019) was

$$\Phi(\mathbf{r},\mathbf{b}) = \frac{1}{2}\|\mathbf{H}(\mathbf{b}_0)\mathbf{r} - \mathbf{I}(\mathbf{b}_0) - \mathbf{W}(\mathbf{b}_0)(\mathbf{b}-\mathbf{b}_0)\|_2^2 - \frac{\lambda}{2}\|\mathbf{I}(\mathbf{b})\|_2^2, \tag{4}$$

where $\mathbf{W}(\mathbf{b}_0)$ is the wave-equation migration velocity analysis operator (WEMVA) evaluated at the wrong background. The reason for proposing such expression was because in the original LWIVU objective function,

$$\Phi(\mathbf{r},\mathbf{b}) = \frac{1}{2}\|\mathbf{H}(\mathbf{b}_0)\mathbf{r} - \mathbf{I}(\mathbf{b}_0) - \mathbf{W}(\mathbf{b}_0)\boldsymbol{\Delta}\mathbf{b}\|_2^2 - \frac{\lambda}{2}\|\mathbf{W}(\mathbf{b}_0)\boldsymbol{\Delta}\mathbf{b} + \mathbf{I}(\mathbf{b}_0)\|_2^2, \tag{5}$$

it was detected that the second term (not including the minus sign) is not concave, as it was expected. In fact, it is convex. The correction consisted in going from equation (5) to (4) by removing the linearization from the second term, which makes it indeed concave (numerical examples supporting this claim are provided in Cabrales-Vargas and Sarkar (2019)).

Equation (1) avoids the linearization of the migration image in both members of the objective function. The main advantages with respect to equation (4) are 1) equation (1) yields a more accurate result because it avoids a numerical approximation of the migration image, and 2) it makes possible to reduce computational operations during the gradient calculation.

To illustrate the second advantage of implementing equation (1) we obtain the corresponding gradient,

$$\nabla\Phi = \begin{bmatrix} \mathbf{H}_0^{\mathrm{T}}\big[\mathbf{H}_0\mathbf{r} - \mathbf{I}(\mathbf{b})\big] \\ -\mathbf{W}(\mathbf{b})^{\mathrm{T}}\big[\mathbf{H}_0\mathbf{r} - \mathbf{I}(\mathbf{b})\big] - \lambda\mathbf{W}(\mathbf{b})^{\mathrm{T}}\mathbf{I}(\mathbf{b}) \end{bmatrix} \tag{6}$$

and reorder terms

$$\nabla\Phi = \begin{bmatrix} \mathbf{H}_0^{\mathrm{T}}\big[\mathbf{H}_0\mathbf{r} - \mathbf{I}(\mathbf{b})\big] \\ -\mathbf{W}(\mathbf{b})^{\mathrm{T}}\big[\mathbf{H}_0\mathbf{r} - \mathbf{I}(\mathbf{b})(1+\lambda)\big] \end{bmatrix}. \tag{7}$$

In the last expression it becomes evident that the adjoint WEMVA operator needs be applied only once each gradient computation. If we instead use equation (6) directly, thus regarding the second member as a regularization term, the WEMVA operator would need to be applied twice.

It is worth understanding the role of each term in equations (1). The first term aims to fit the migration image to the reflectivity, the latter under the action of the Hessian. In other words, this term alone performs linearized waveform inversion (LWI) in model domain. However, in contrast with the conventional inversion for reflectivity, the migration image does not remain unchanged. It gets updated when the background model is updated, driven to maximizing its energy by the second term in equation (1).

## NUMERICAL RESULTS

I test the JIRB method on the sedimentary sector of the SigsbeeA model. The true background model has a Gaussian high-velocity anomaly added with a maximum of approximately 900ft/s, whilst the wrong background model does not include the anomaly. In slowness squared the anomaly becomes negative (Figure 1).

I synthesized data using acoustic Born modeling with the true background model. Figure 2 shows the true reflectivity that I also used for the computation of the data (the six spikes are part of the reflectivity model; they are not related to the point-spread functions mentioned later). For all the inversion tests I employed the wrong model, except for the control reflectivity image computed for comparison purposes.

The amplitudes of the following figures are displayed on the same color scale. I used linearized waveform inversion (LWI) with a linear conjugate gradient solver to invert for the reflectivity, assuming a fixed background model. On the other hand, for nonlinear JIRB I used the steepest descent method with a parabolic line search. The inversions were run for 18 iterations. I set this limit because the JIRB numerical experiment stopped there after being unable to find a suitable step size.

Figure 3 shows the LWI control result using the true background model. The FWI Gauss-Newton Hessian was pre-computed using point-spread functions according to Fletcher et al. (2016). The estimated Hessian is interpolated and applied "on the fly".

Figure 4 shows the result of LWI using the wrong background model. As expected, not accounting for the positive anomaly in velocity (negative anomaly in slowness squared) produces a pull-up at the middle of the section. Compare the position of reflections and the spike in the central region with Figures 2 and 3. The shift is subtle. Finally, Figure 5 shows the JIRB result, using as initial model a zero reflectivity and the wrong background. Notice that the reflectors have been moved to their correct position. I used $\lambda = 12$ for the inversion, which I obtained by trial and error. Also notice that the corresponding normalized objective function has negative values. The reason is that the relatively large value of $\lambda$ makes the second member of equation (1) more prominent, and this one is expected to become more negative with the iteration number. The objective functions for each member of JIRB are shown in Figure 6.

For better visualization Figure 7 compares zooms at the center of the three sections. The LWI result with the wrong background (Figure 7a) has the central spike and other features pulled upwards with respect to the horizontal grid lines. Compare with LWI using the true background and JIRB (Figures 7b and 7c, respectively).

For the sake of completeness, Figure 8 shows the perturbation in the background obtained with JIRB (subtracting the wrong background model from the inverted background model) and the true perturbation. They are plotted using the same color scale.

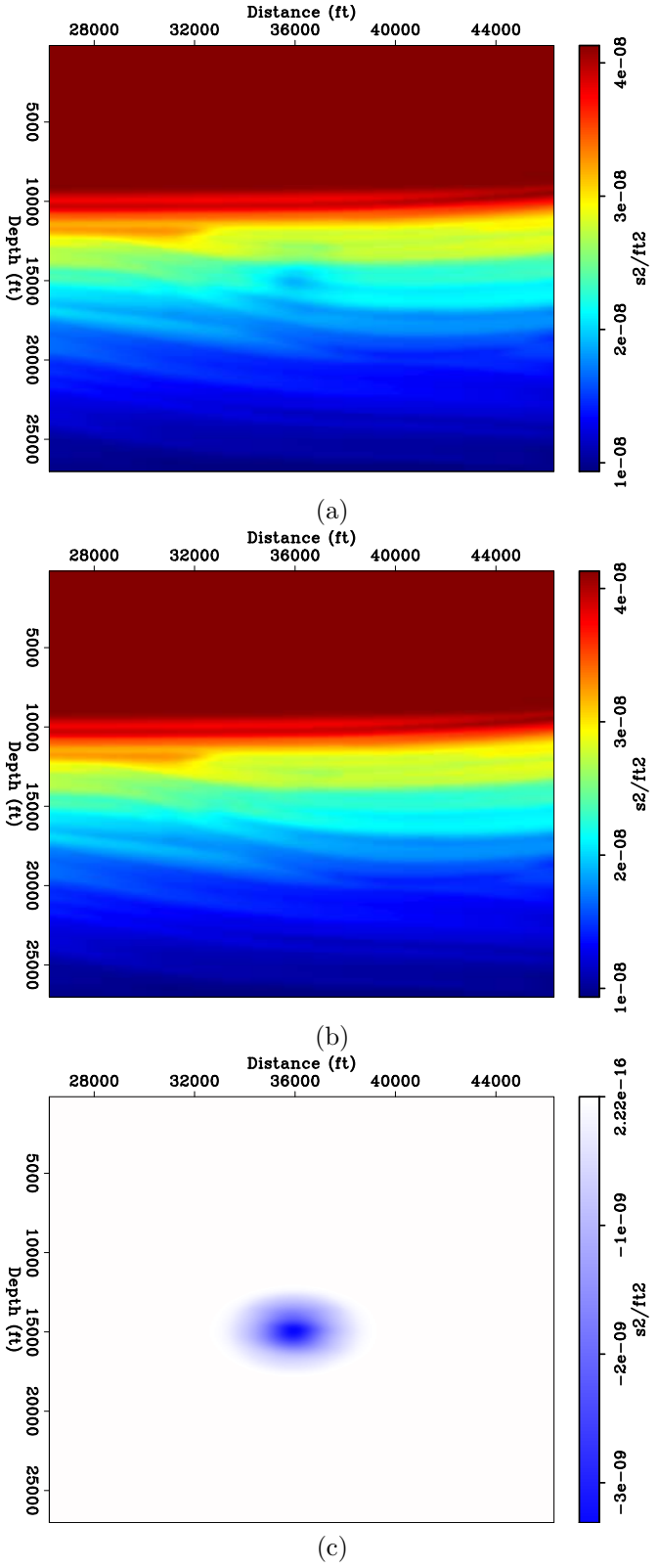


Figure 1: Section of SigsbeeA model in slowness squared: a) True background model; b) Wrong background model; c) Gaussian anomaly. [**ER**]

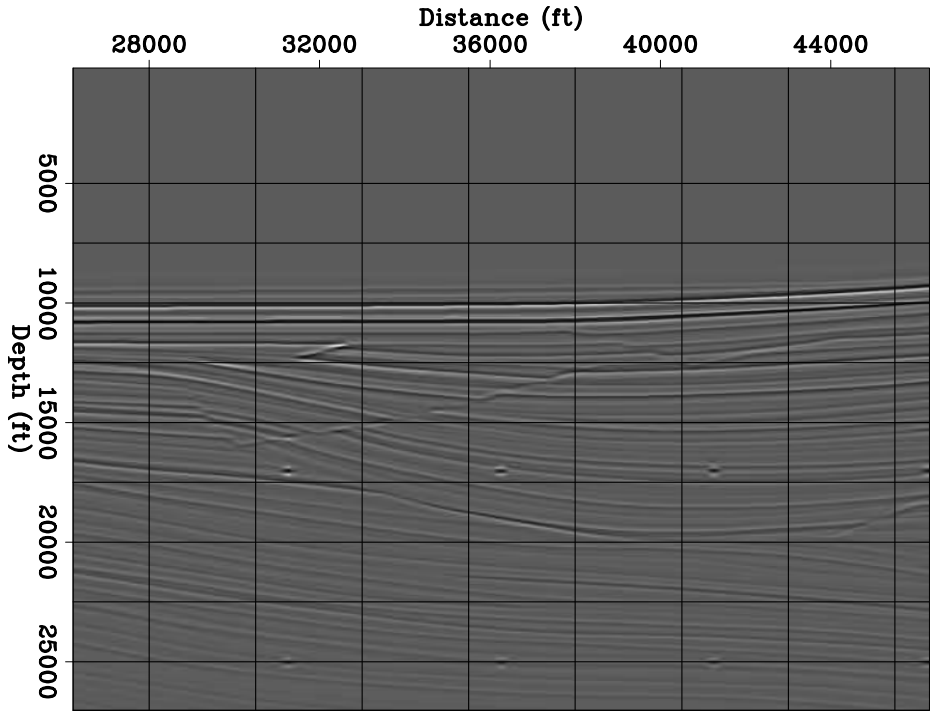


Figure 2: Subsurface reflectivity of the Sigsbee model. [**ER**]

## CONCLUSION

The numerical results show that the JIRB algorithm achieves the goal of correcting the inverted reflectivity whilst inverting for the background model, particularly in terms of kinematics. However, the overall amplitude of the reflectivity section is higher in comparison to LWI. One possible explanation is that, having expanded the model space by incorporating the background model, the corresponding null space also expanded. New experiments incorporating minimum norm regularization can be used to correct the amplitudes of reflectivity.

The next step will be adapting the 3D codes to perform JIRB for the application to field data.

## ACKNOWLEDGEMENT

I would like to thank Petróleos Mexicanos for having financed my studies for five years. I also would like to thank Rahul Sakar, who massively contributed to the current implementation of this methodology.

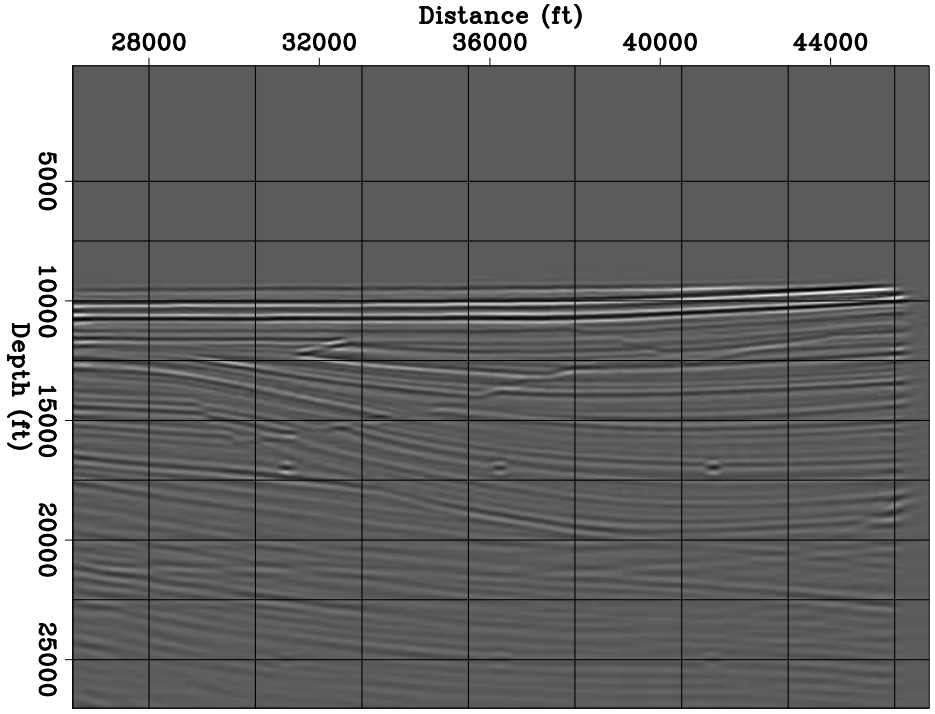


(a)

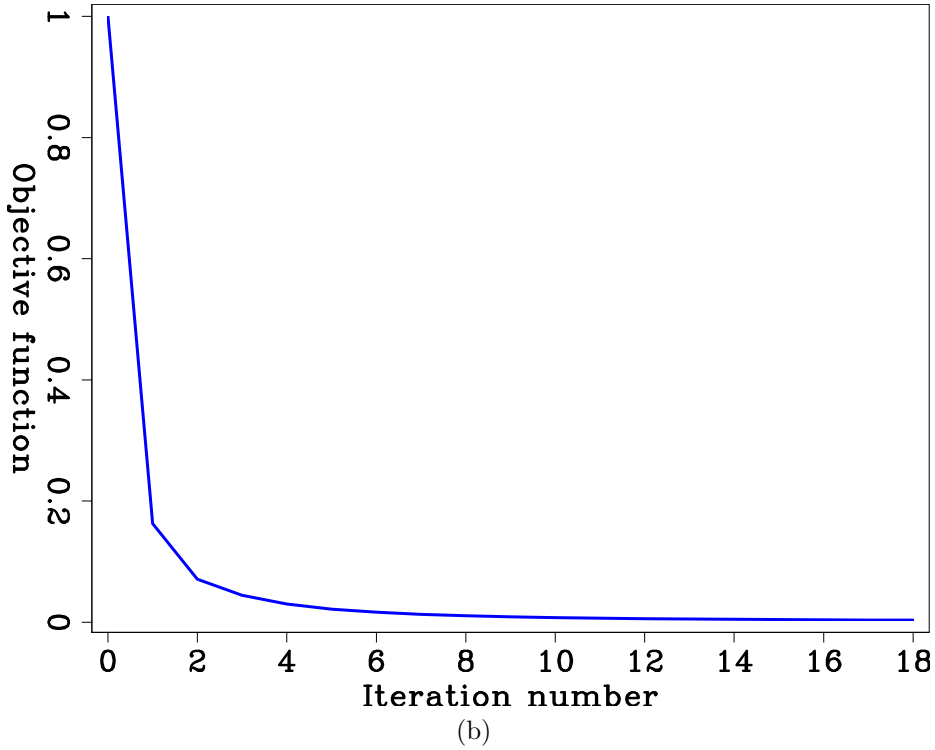


(b)

Figure 3: a) Inverted reflectivity using LWI with the true background model. b) Normalized objective function. [**CR**]

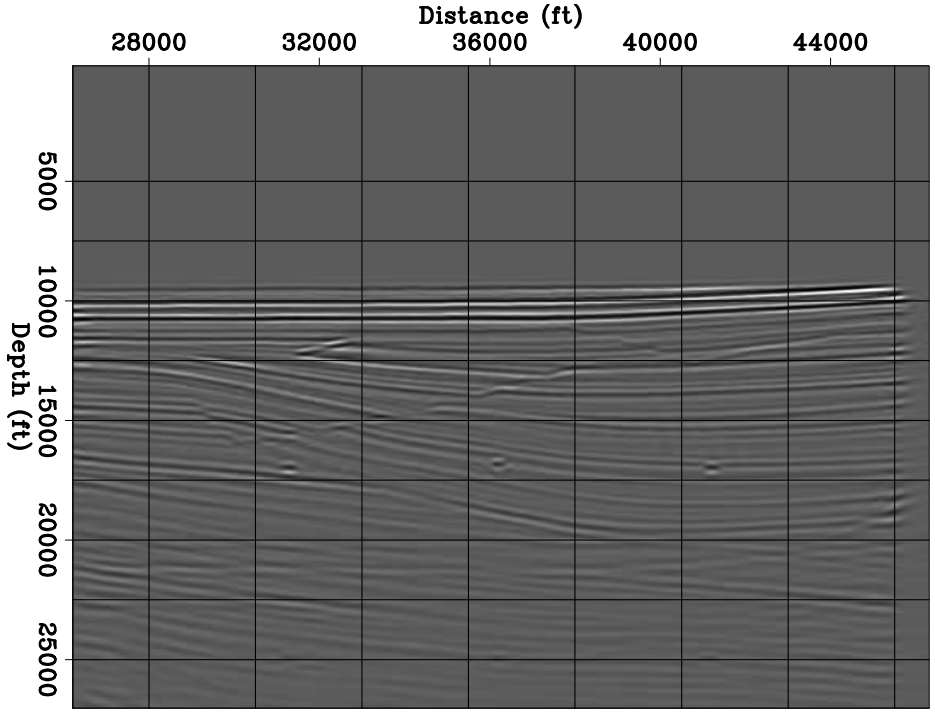


(a)

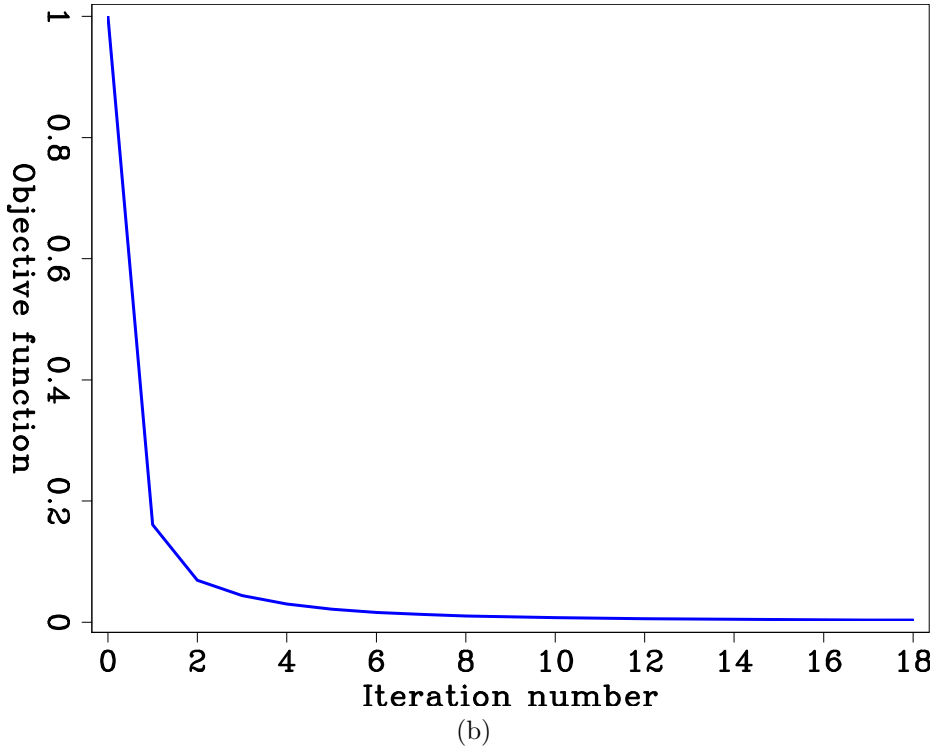


(b)

Figure 4: a) Inverted reflectivity using LWI with the wrong background model. b) Normalized objective function. [**CR**]

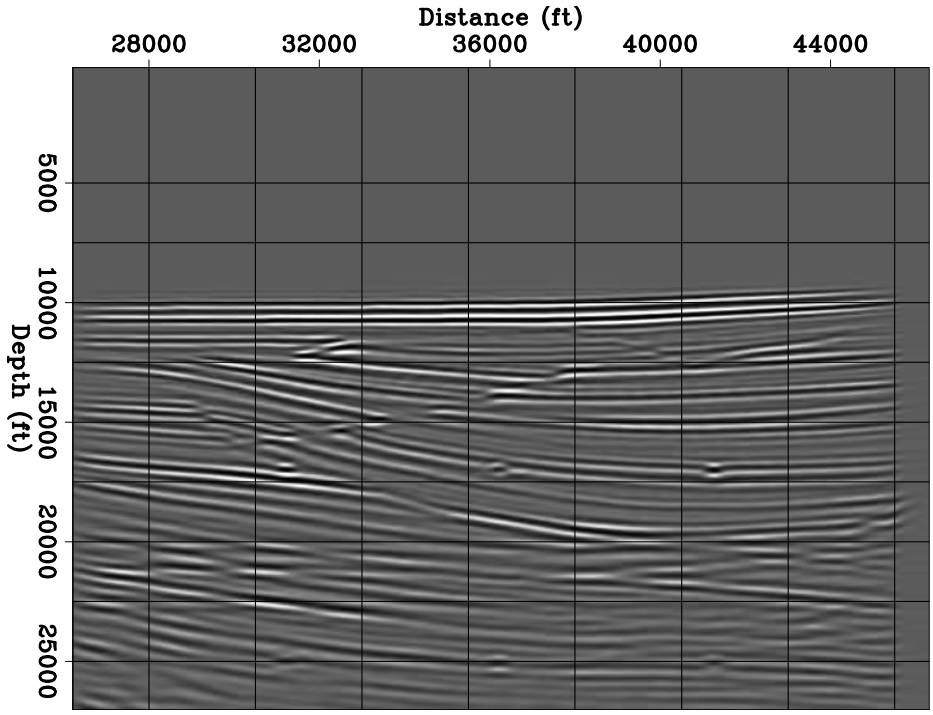


(a)

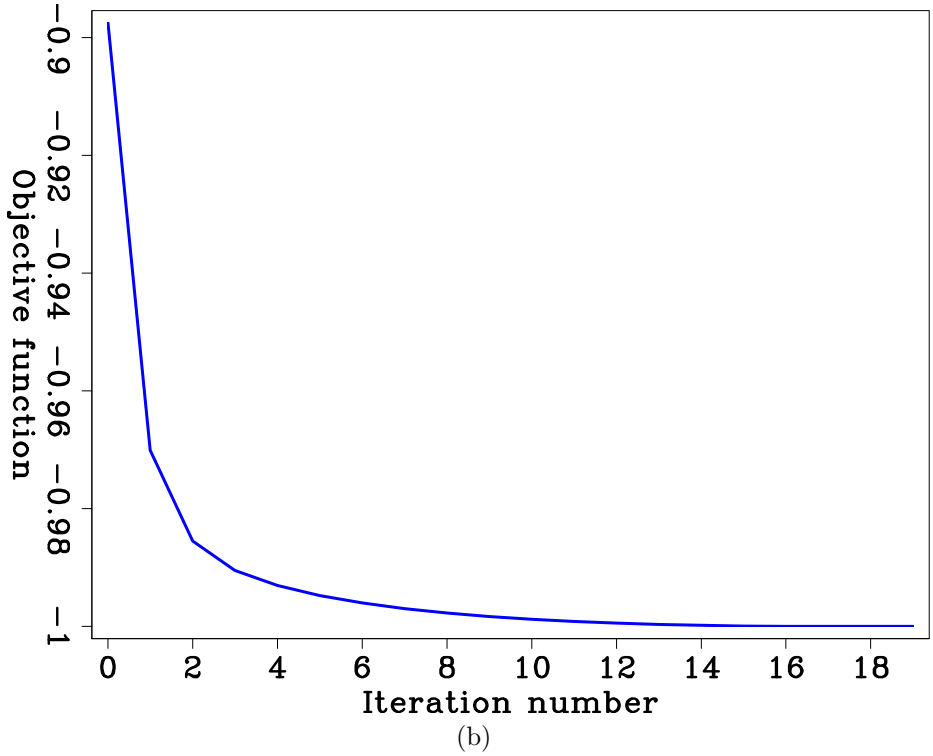


(b)

Figure 5: a) Inverted reflectivity using JIRB with the wrong background model. b) Normalized objective function [**CR**]

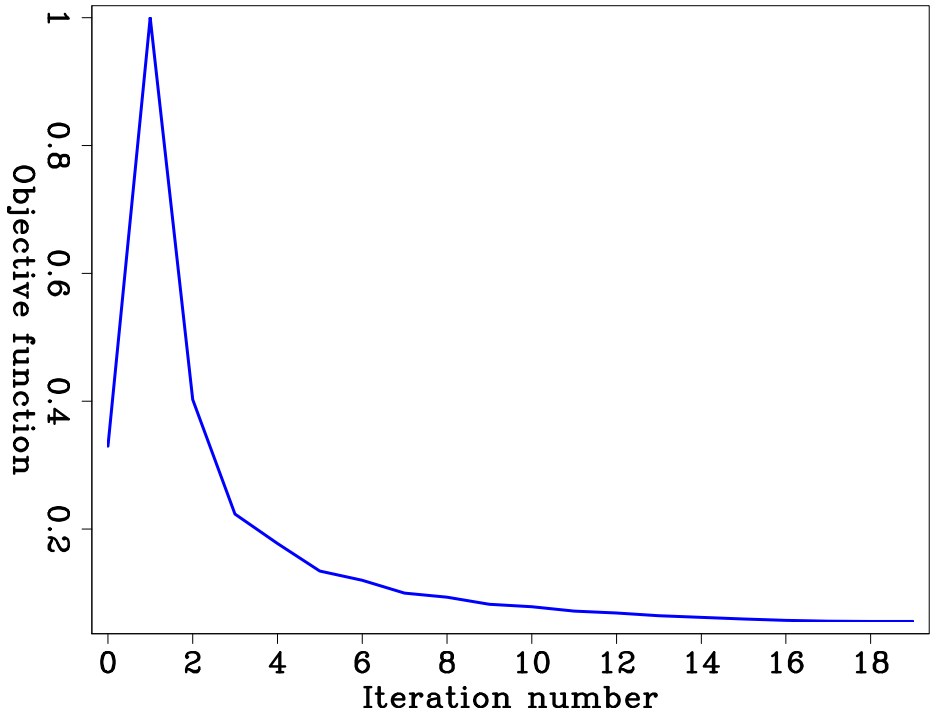


(a)

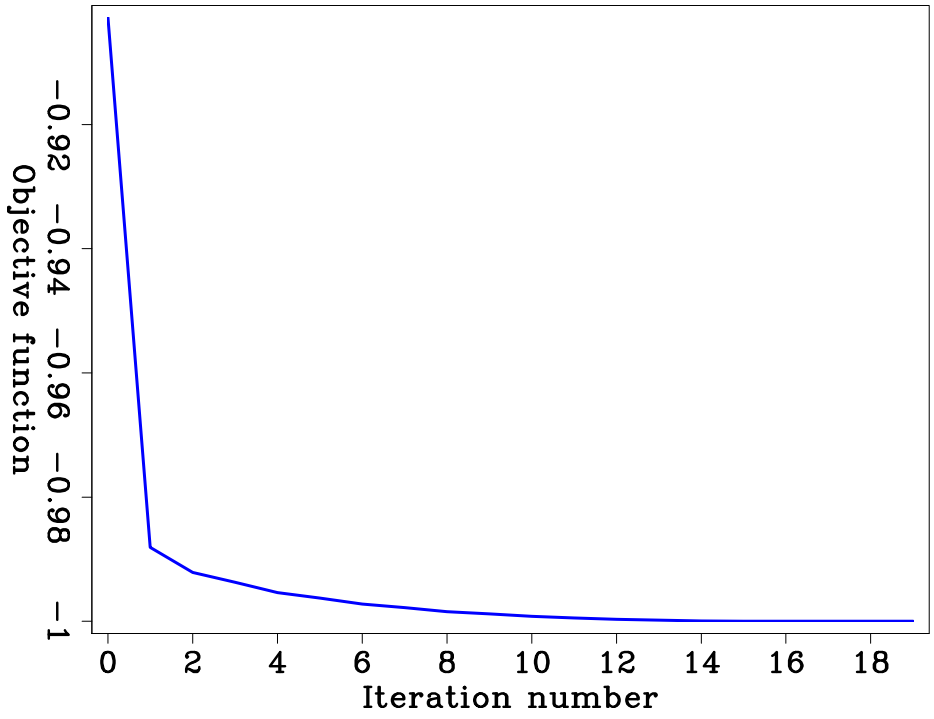


(b)

Figure 6: a) First member of JIRB normalized objective function: $\|\mathbf{H}(\mathbf{b}_0)\mathbf{r} - \mathbf{I}(\mathbf{b})\|_2^2$. b) Second member of JIRB normalized objective function: $-\|\mathbf{I}(\mathbf{b})\|_2^2$. [**CR**]

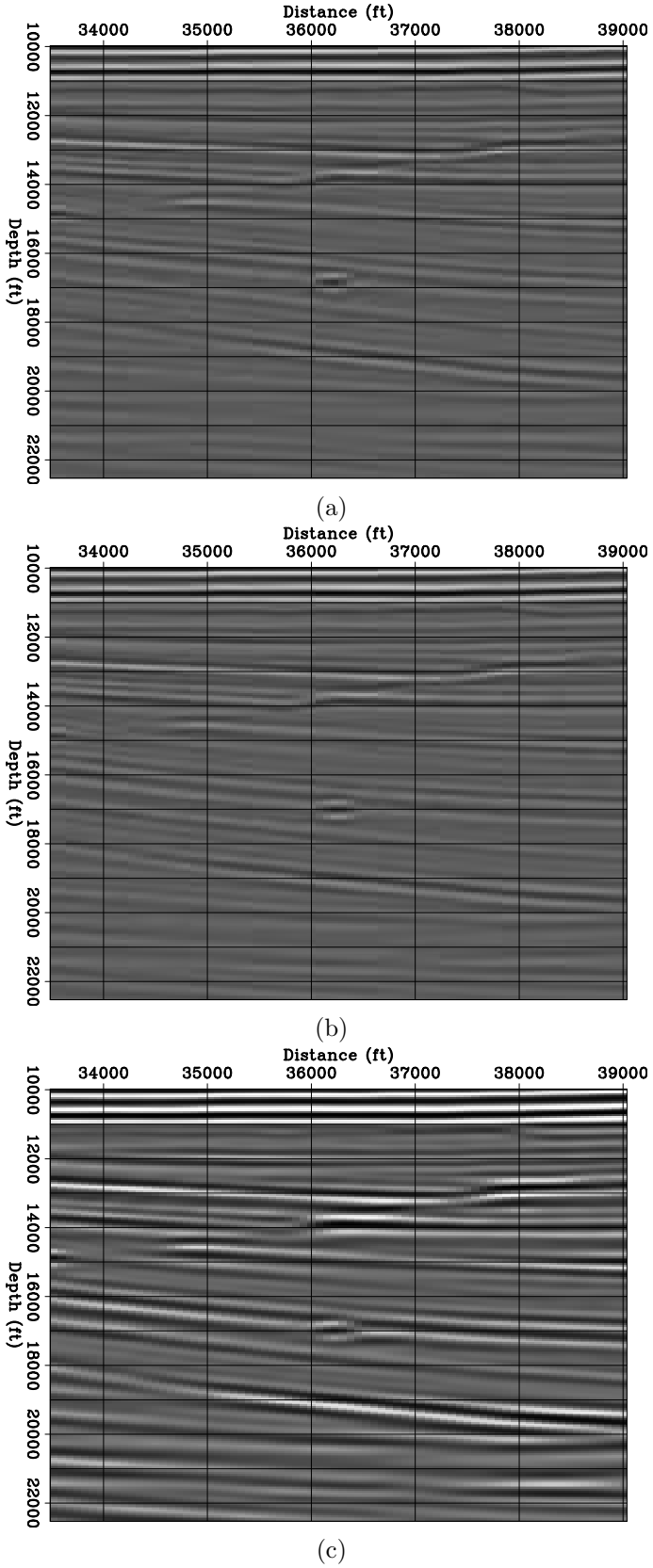


Figure 7: Zoom to the central parts of the reflectivity estimations with a) LWI with the wrong background, b) LWI with the true background, and c) JIRB. [**CR**]

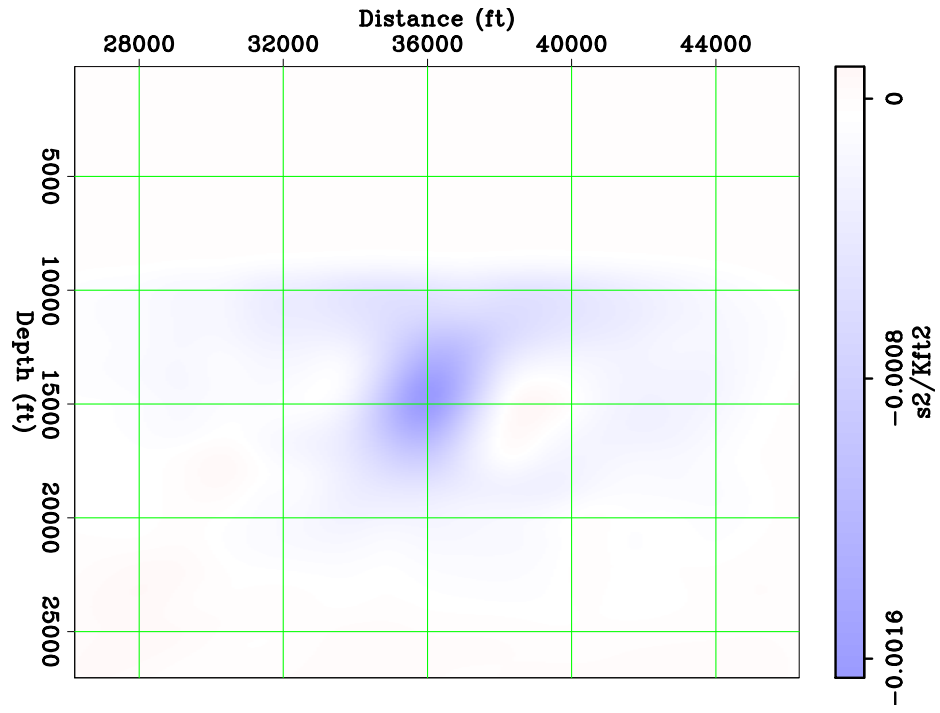


(a)

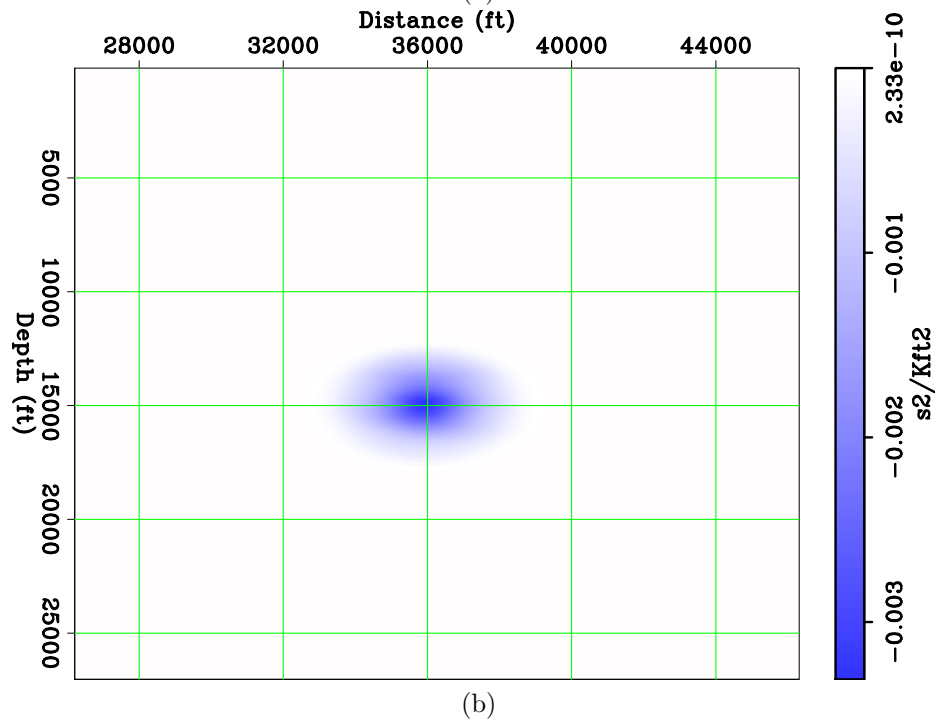


(b)

Figure 8: Comparison between a) perturbation in the background obtained with JIRB, and b) true perturbation in the background model. [**CR**]

# REFERENCES

Cabrales-Vargas, A., 2017, Implementing Wave-Equation Migration Velocity Analysis Within Linearized Waveform Inversion with Velocity Updating: Considerations and Challenges : SEP-Report, **170**, 149–156.

———, 2018, Improving reflectivity using linearized waveform inversion with velocity updating: SEP-Report, **172**, 193–208.

Cabrales-Vargas, A., B. Biondi, and R. Clapp, 2017, Our progress towards linearized waveform inversion with velocity updating (LWIVU): SEP-Report, **168**, 151–162.

Cabrales-Vargas, A. and R. Sarkar, 2019, A nonlinear scheme to perform linearized waveform inversion with velocity updating: SEP-Report, **176**, 85–100.

Fletcher, R., D. Nichols, R. Bloor, and R. Coates, 2016, Least-squares migation - data domain versus image domain using point spread functions: The Leading Edge, **35**, no. 2, 157–162.

Tarantola, A., 1984, Inversion of seismic reflection data in the acoustic approximation: Geophysics, **49**, 1259–1266.

Virieux, J. and S. Operto, 2009, An overview of full-waveform inversion: Geophysics, **74**, no. 6, WCC1–WCC26.

## REFERENCES

Cabrales-Vargas, A., 2017, Implementing Wave-Equation Migration Velocity Analysis Within Linearized Waveform Inversion with Velocity Updating: Considerations and Challenges : SEP-Report, **170**, 149–156.

———, 2018, Improving reflectivity using linearized waveform inversion with velocity updating: SEP-Report, **172**, 193–208.

Cabrales-Vargas, A., B. Biondi, and R. Clapp, 2017, Our progress towards linearized waveform inversion with velocity updating (LWIVU): SEP-Report, **168**, 151–162.

Cabrales-Vargas, A. and R. Sarkar, 2019, A nonlinear scheme to perform linearized waveform inversion with velocity updating: SEP-Report, **176**, 85–100.

Fletcher, R., D. Nichols, R. Bloor, and R. Coates, 2016, Least-squares migation - data domain versus image domain using point spread functions: The Leading Edge, **35**, no. 2, 157–162.

Tarantola, A., 1984, Inversion of seismic reflection data in the acoustic approximation: Geophysics, **49**, 1259–1266.

Virieux, J. and S. Operto, 2009, An overview of full-waveform inversion: Geophysics, **74**, no. 6, WCC1–WCC26.